Microelectronics Reliability 125 (2021) 114345

Contents lists available at ScienceDirect

Microelectronics Reliability

journal homepage: www.elsevier.com/locate/microrel

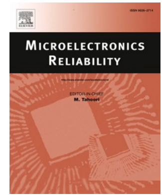

Temperature-dependent electrical characteristics of neutron-irradiated GaN Schottky barrier diodes

Min Zhu [a,d,g,1], Yuan Ren [b,f,1], Leidang Zhou [c], Jiaxiang Chen [a,d,g], Haowen Guo [a], Liqi Zhu [a], Baile Chen [a], Liang Chen [e], Xing Lu [b,*], Xinbo Zou [a,*]

[a] *School of Information Science and Technology, ShanghaiTech University, 201210 Shanghai, China*
[b] *State Key Laboratory of Optoelectronic Materials and Technologies, School of Electronics and Information Technology, Sun Yat-sen University, 510006 Guangzhou, China*
[c] *School of Microelectronics, Xi'an Jiaotong University, 710049 Xi'an, China*
[d] *Shanghai Institute of Microsystem and Information Technology, Chinese Academy of Sciences, 200050 Shanghai, China*
[e] *State Key Laboratory of Intense Pulsed Radiation Simulation and Effect, Northwest Institute of Nuclear Technology, Xi'an 710024, China*
[f] *Institute of Semiconductors, Guangdong Academy of Sciences, 510650 Guangzhou, China*
[g] *University of Chinese Academy of Science, 100049 Beijing, China*

A R T I C L E I N F O

Keywords:
Deep level traps
GaN Schottky barrier diode
Low frequency noise
Neutron irradiation

A B S T R A C T

Temperature-dependent electrical characteristics were explicitly investigated for a 400-μm diameter neutron-irradiated (NI) GaN Schottky barrier diode (SBD). Based on *C-V* measurements, a marked decrease in electron concentration has been revealed for the NI diode compared with the pristine sample, suggesting a thermal-enhanced carrier removal effect. Neutron irradiation causes noticeable Schottky barrier height inhomogeneity, which was studied by a two-barrier model. Data indicates that neutron irradiation affects a small but measurable suppression of leakage current as well as low frequency noise level. Despite a new deep-level trap was identified, the temperature-dependent electrical results specified GaN SBD's outstanding resistance to neutron irradiations and robustness in extreme operation temperatures.

1. Introduction

Energetic particles, including neutrons [1–4], are naturally observed in space environment and could be artificially generated by various neutron sources. 14 MeV neutron beams, with high energy and good penetrability, have been regarded as a powerful tool in non-destructive test of materials [5] and medical treatment [6,7]. To facilitate inclusion of electronics in those neutron radiation environments, it is demanding to have vigorous semiconductor devices to withstand high-energy neutron irradiations [8], expanding functional life time of electronic devices in aerospace craft, avionics systems, medical equipment, and so on.

III-N semiconductors have received immense research interest for high power [9], high frequency [10] and optoelectronic applications, owing to their superior material properties, including wide energy bandgap, high electron velocity, and large critical electric field. In addition, the outstanding chemical stability of III-N materials, as a result of strong bonding strength and high displacement threshold energy [11], has enabled GaN-based devices suitable for various radiative environments [12–17].

There have been some studies performed towards understanding how neutron irradiation affects GaN material properties [18,19]. Typically, neutron irradiation would induce structural defects in GaN-based materials, and the irradiation-induced dislocations would propagate to the material surface and cause surface morphology deterioration [20]. Rutherford backscattering and high resolution X-ray diffraction were employed to characterize defects in GaN films after irradiations [21]. Using thermally stimulated current method, neutron irradiation induced defects, particularly electrically-active defects in GaN film were investigated [22]. In addition, the conductivity of p-type GaN material was found to be compromised due to carrier compensation caused by neutron irradiation. As the compensation effect was strengthened, the p-type GaN samples could even be converted to highly resistive n-type materials [23].

* Corresponding authors.
E-mail addresses: lux86@mail.sysu.edu.cn (X. Lu), zouxb@shanghaitech.edu.cn (X. Zou).
[1] M. Zhu and Y. Ren contributed equally to this work.

https://doi.org/10.1016/j.microrel.2021.114345
Received 3 March 2021; Received in revised form 3 August 2021; Accepted 15 August 2021
Available online 26 August 2021
0026-2714/© 2021 Published by Elsevier Ltd.

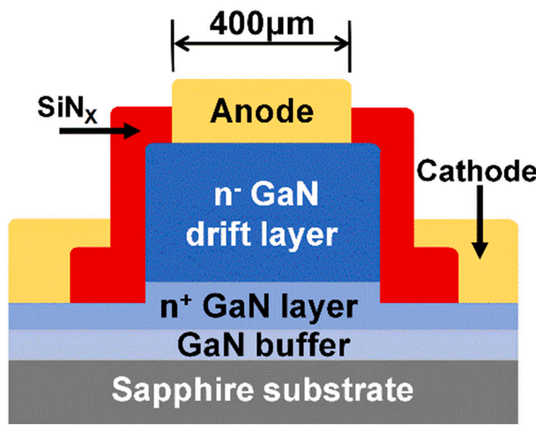

Fig. 1. Cross-sectional view of GaN quasi-vertical Schottky barrier diode.

However, there are only a few reports devoted to the impact of neutron irradiation on GaN-based devices. Carrier removal effect [24,25] and forward current degradation [26,27] induced by irradiations have been reported for GaN-based diodes. Upon neutron irradiation, deep-level defects and thus a reduction of two-dimensional electron gas concentration have been revealed for hetero-structure based devices [28,29]. One of our previous works [26] reported 14.9 MeV neutron irradiation effects on Ni/GaN Schottky contacts with different irradiation influence. Nevertheless, explicit investigations of electrical characteristics at low temperatures and their temperature dependence are still unclear. The lack of such results and analysis would mask the potential of employing GaN-based devices for deep space explorations where cryogenic temperature and high energy particles may simultaneously exist. In this paper, temperature-dependent current-voltage (*I-V-T*), capacitance-voltage (*C-V-T*) were employed to unveil current conduction and reverse blocking mechanisms of GaN SBD after neutron irradiation. Furthermore, deep-level transient spectroscopy (*DLTS*) and low frequency noise spectroscopy (*LFNS*) were utilized to identify trap and noise features for both pristine and neutron-irradiated (NI) SBDs.

2. Materials and methods

The GaN SBDs (Fig. 1) used in this study were grown on a 2-in. sapphire substrate by metal organic chemical vapor deposition (MOCVD). The epitaxial structure started from a 1-μm thick GaN buffer layer, followed by a 1.8-μm thick n^+-GaN layer with electron concentration of 5×10^{18} cm^{-3}. Finally, a 5.8-μm thick unintentionally-doped n^--GaN layer (with nominal carrier concentration of 5.3×10^{15} cm^{-3}) was grown. The fabrication of GaN SBD began with deposition of SiO_2 by plasma enhanced chemical vapor deposition (PECVD). Then mesa isolation was performed by inductively coupled plasma (ICP) etch using SiO_2 layer as an etching mask. After SiN_x sidewall passivation, Ti/Al/Ni/Au metal stacks and 400-μm diameter Ni/Au Schottky metals serving as the electrodes were deposited on the exposed n^+-GaN layer and mesa. The annealing condition of Ti/Al/Ni/Au Ohmic contact is 850 °C for 30 s, and no annealing was performed for the Ni/Au Schottky contact.

Neutron irradiation experiments were conducted with a 14.9 MeV fast neutron beam (irradiance of 8×10^{14} n cm^{-2}) generated by deuterium-tritium fusion at the K600 Neutron Generator in China Institute of Atomic Energy (CIAE) in Beijing, China. The *I-V-T* and *C-V-T* measurements were implemented at low temperature using cryostat cooled by liquid helium and Keysight B1500A parameter analyzer. The device was further submitted to *DLTS* and *LFNS* analyzer measurement to study trap and noise information.

3. Results and discussion

Fig. 2(a) shows the *C-V* characteristics of pristine and irradiated SBDs, measured at 1 MHz from 100 K to 275 K. The curves of pristine SBD from 100 K to 275 K are overlapped. The capacitance of the NI sample was relatively smaller than the pristine sample at all measurement temperatures. In addition, the slopes of $1/C^2$-V curves were much steeper than the pristine counterpart. The net carrier concentration N_S could be extracted by Eq. (1):

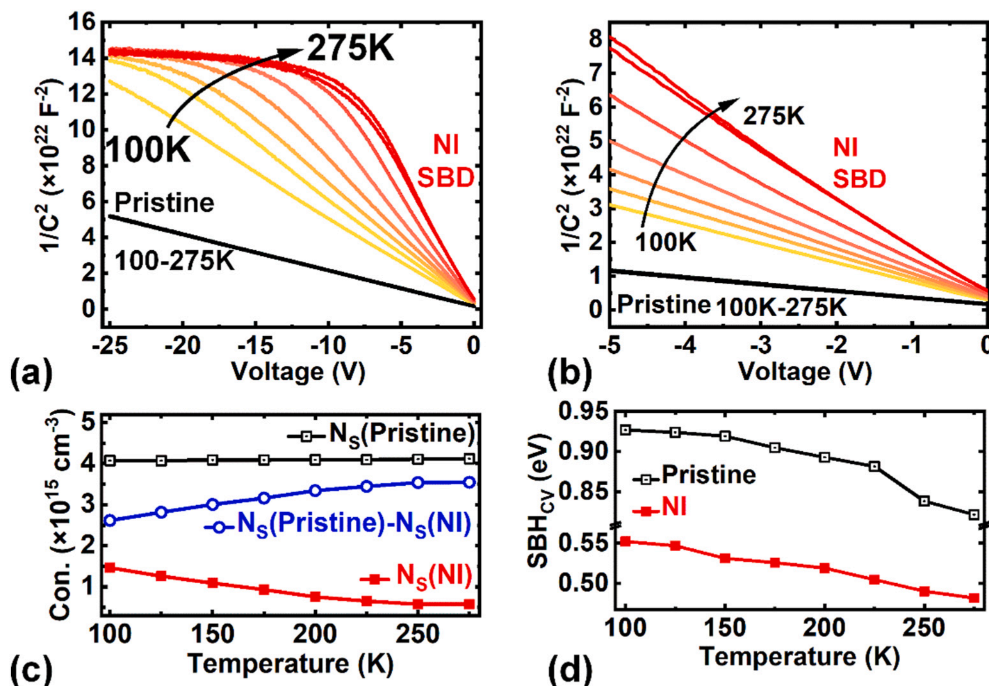

Fig. 2. Temperature-dependent (a) *C-V* characteristics up to -25 V; (b) Zoomed-in *C-V* characteristics from 0 V to -5 V; (c) Net carrier concentration (Con.); (d) Schottky barrier height (SBH_{CV}) of the pristine and NI SBDs from 100 K to 275 K.

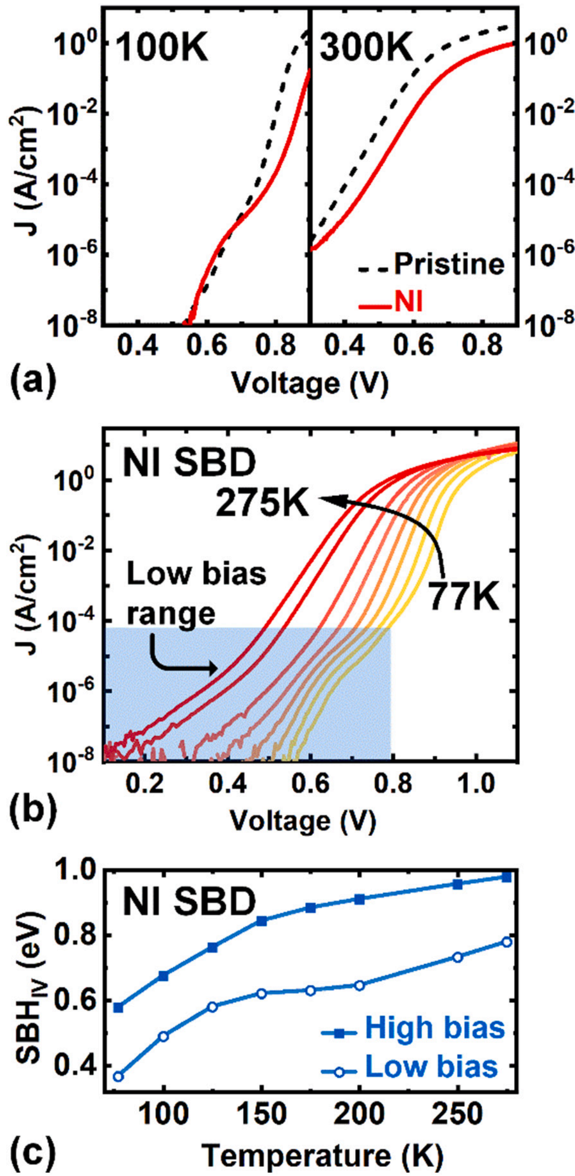

Fig. 3. (a) Forward current density (J) characteristics of pristine and NI SBDs at 100 K and 300 K; (b) *I-V* characteristics of NI GaN SBD from 77 K to 275 K; (c) Extracted Schottky barrier heights (SBH_{IV}) from high/low bias region as a function of temperature.

$$\frac{1}{C^2} = \frac{2}{\varepsilon_0 \varepsilon_s q F^2 N_S}\left(V_{bi} - \frac{k_B T}{q} - V\right) \quad (1)$$

where F is the area of device, V_{bi} is built-in potential, ε_0 is the permittivity in vacuum, ε_s is the relative dielectric constant of GaN, respectively. Fig. 2(c) shows a lower N_S value from the irradiated diode compared with the pristine sample, suggesting a new acceptor level in the NI-sample and thus a carrier concentration compensation effect. At 100 K, the extracted net carrier concentration was reduced from original 4.07×10^{15} cm^{-3} to 1.46×10^{15} cm^{-3} for GaN SBD after fast neutron radiation. From 100 K to 275 K, the net carrier concentration in the NI-sample was further reduced to 0.57×10^{15} cm^{-3}. The reduction of N_S of NI SBD implied a thermal-enhanced carrier removal effect [30].

Schottky barrier height (SBH) ϕ_{B-CV} could be obtained by Eqs. (1) and (2).

$$q\phi_{B-CV} = qV_{bi} + (E_C - E_F) + k_B T \quad (2)$$

where E_C and E_F denote conduction band minimum and Fermi level, respectively.

For NI SBD, with reduction of N_S upon neutron irradiation, qV_{bi} which denotes the Fermi level difference between metal and semiconductor would be shrunk significantly compared with that of pristine SBD. Though $(E_C - E_F) = kT \ln(N_C/N_S)$ of NI SBD holds a slight increase as N_S decreases, $q\phi_{B-CV}$ of NI-SBD is still lower than that of pristine diode overall. The $q\phi_{B-CV}$ is slightly decreased by 110 meV (for pristine SBD) and 70 meV (for NI SBD) as increasing temperature from 100 K to 275 K, as shown in Fig. 2(d) [31,32].

Fig. 3(a) shows forward *I-V* characteristics of pristine and NI diodes. Compared with the pristine diode, the forward current density of NI SBD was compromised by around 20% at room temperature or lower temperatures. Detailed *I-V-T* characteristics of the NI SBD were shown in Fig. 3(b). At all temperature steps, the NI sample exhibited two regions of linearity and suggested two barrier heights [33–36]. Low- and high-barrier height could be separately extracted by thermionic emission (TE) model as described by Eq. (3).

$$J_{TE} = A^* T^2 exp\left(\frac{-q\phi_{B-IV}}{k_B T}\right)\left[exp\left(\frac{qV}{nk_B T}\right) - 1\right] \quad (3)$$

where A^* is Richardson constant, with a value of 26.5 A cm^{-2} K^{-2} [37], $q\phi_{B-IV}$ is the Schottky barrier height, V is the forward applied bias, and n is the ideality factor. From 77 K to 275 K, the low- and high- barrier heights were both increased for the NI-sample, from 0.37 eV to 0.78 eV, and from 0.58 eV to 0.98 eV, respectively.

In this TE model, the current transport of electrons across the interface between semiconductor and metal is a thermally-activated process. At low temperatures, current transport will be dominated by carrier flowing through the lower part of inhomogeneous SBH [38–41]. As increasing the temperature, more electrons have sufficient energy to surmount the higher part of SBH, resulting an increase of effective Schottky barrier height as the temperature.

It should be also noted that when $T < 150$ K, the low and high barrier heights (extracted from low- and high- bias region respectively) for the NI and pristine samples were quite comparable to each other (shown in the supplementary material). As temperature was over 150 K and the net carrier concentration of the NI sample was further reduced, two barriers were kept being observed for the NI-sample, but only one barrier was identified for the pristine sample. This comparison concludes that the two-barrier phenomenon was augmented by neutron irradiation. The existence of the two barriers at all temperature steps reflects the spatial inhomogeneity of barrier height across the metal/semiconductor interface upon neutron irradiation.

Fig. 4(a) shows the leakage current density of pristine and NI diodes at 300 K and 77 K. Statistically, the average reverse current of the NI SBD was slightly lower than that of the pristine samples [27]. The reverse current density of the NI-sample was re-plotted in Fig. 4(b) and (c) that the electrical field and temperature dependent leakage current could be well explained by the Poole-Frenkel emission (PFE) model.

$$J_{PF} = C' E \, exp\left[-\frac{q}{k_B T}\left(\phi_T - \sqrt{\frac{qE}{\pi \varepsilon_0 \varepsilon_s}}\right)\right] \quad (4)$$

where C' is a constant, E is the electric field in the semiconductor layer, $q\phi_T$ denotes the effective barrier height of electron emission from trap state.

Fig. 4(b) shows linear dependence of $Ln(J/E)$ on $E^{1/2}$ at all measurement temperatures from 77 K to 300 K. Using Poole-Frenkel emission model, the effective barrier height or activation energy $q\phi_T$ could be extracted, 0.18 eV for NI SBD while 0.11 eV for the pristine SBD. Upon neutron irradiation, a larger activation energy was obtained for NI-SBD, suggesting a larger barrier height to overcome for electron emission, in a good agreement with the reduced leakage current measured. Similar correlations between activation energies and leakage current have been reported in the literature [42–44]. Fig. 4(c) illustrated that for a fixed

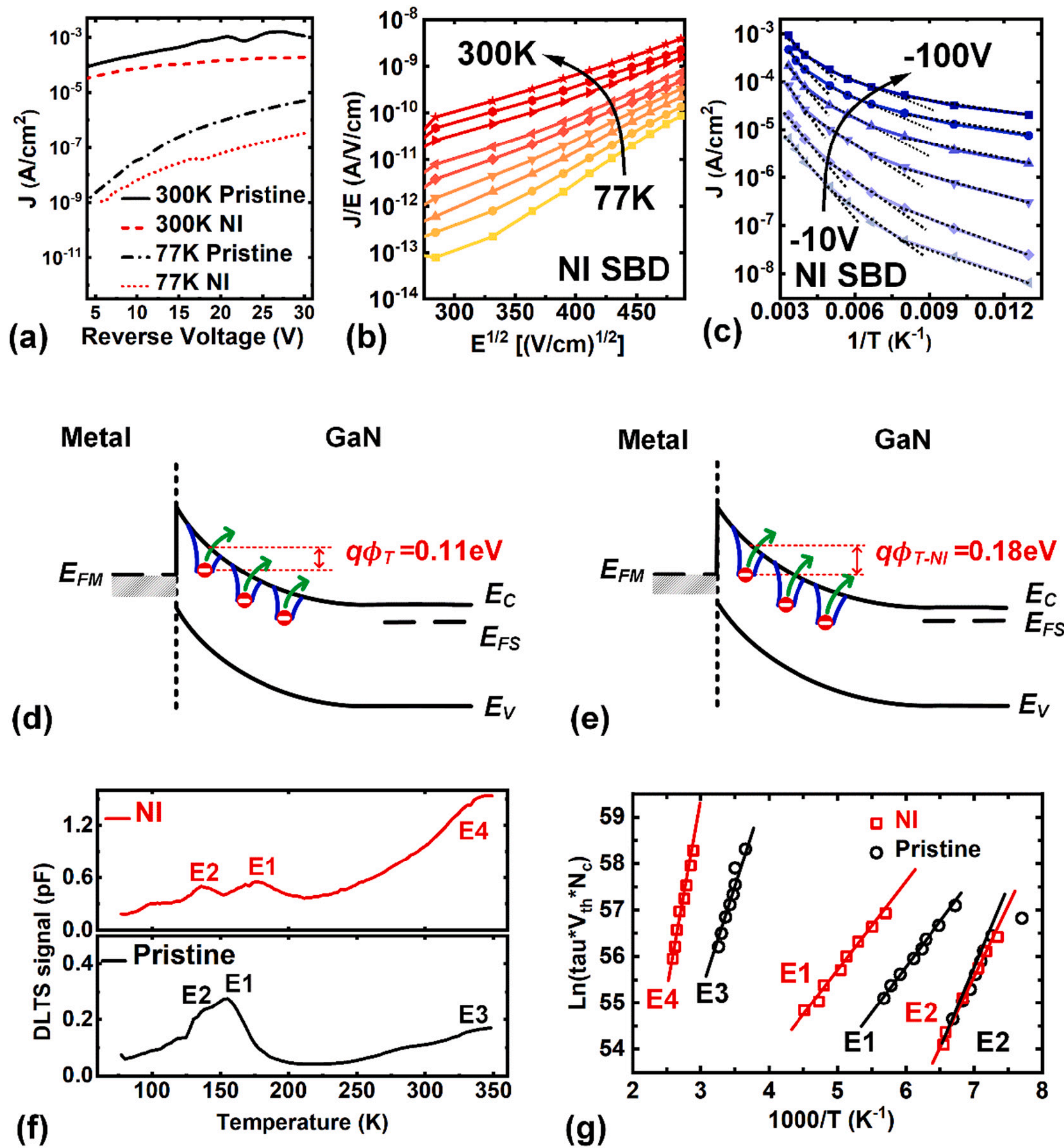

Fig. 4. (a) Comparison of reverse current between pristine and NI SBDs at 77 K and 300 K; (b) $Ln(J/E)$ versus $E^{1/2}$ from 77 K to 300 K; (c) Leakage current density as a function of $1/T$ with the reverse bias from −10 V to −100 V; Illustration of Poole-Frenkel effect for (d) pristine SBD and (e) NI SBD; (f) *DLTS* spectra of pristine and NI SBDs from 77 K to 350 K; (g) Arrhenius plot of three electron traps for each sample.

Table 1
Detailed *DLTS* results including activation energy, capture cross section and trap concentration.

		E_C-E_T (eV)	σ (cm^2)	N_T ($\times 10^{14}$ cm^{-3})
Pristine	E1	0.144	1.06×10^{-21}	1.16
	E2	0.266	2.87×10^{-15}	0.61
	E3	0.468	1.78×10^{-17}	0.58
NI	E1	0.149	3.50×10^{-21}	1.60
	E2	0.254	6.44×10^{-16}	1.40
	E4	0.640	9.77×10^{-17}	5.06

reverse bias at various temperatures, the curves representing the leakage current consist of multiple segments with various steepness, which corresponded to contributions from multi trap states with discrete activation energies.

Fig. 4(d) and (e) illustrate Poole-Frenkel effect for pristine and NI SBD, respectively. E_C, E_V, E_F denote the edge of conduction band, the edge of valence band, and the Fermi level, respectively. When an electrical field applied to the SBD, the electrons captured by trap states would become more likely to get de-trapped to the conduction band as shown in the energy diagram [45].

To locate and compare the deep level traps in both diodes, *DLTS* spectra were employed. Fig. 4(f) shows the *DLTS* spectra of the two samples recorded with a reverse bias $V_R = -6$ V, a filling pulse height $V_P = -1$ V and a filling pulse width $t_P = 100$ ms. The extracted trap information was summarized in Table 1.

The origins of traps E1 and E2 have been presumed to be associated with oxygen impurities or nitrogen vacancy [46–48]. After neutron irradiation, increased trap concentration (N_T) was found for these two trap levels. Upon irradiation, a newly-found deep-level trap E4, 0.64 eV under the conduction band minimum was spotted for the NI SBD [11], in a good agreement with trap level (E_C-0.65 eV) identified for a neutron irradiated GaN SBD in the literature [20] although E3 in the pristine sample was not observed any more.

Fig. 5(a) shows the representative noise spectra under reverse bias for a wide temperature range from 50 K to 350 K. At a fixed -9 V, the device was reverse biased that the low-frequency noise performance for a depleted region could be revealed. The noise power spectral density

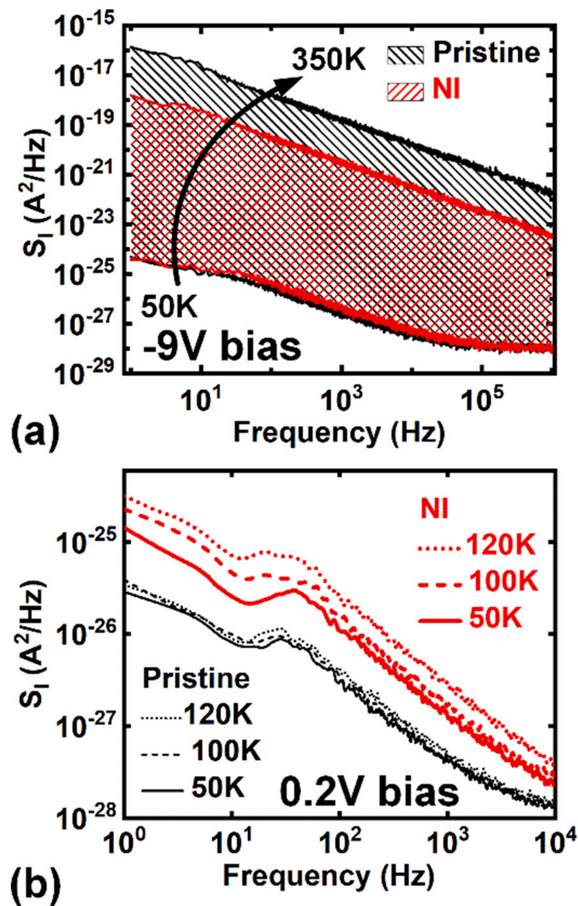

Fig. 5. (a) Noise spectra at reverse bias from 50 K to 350 K; (b) Lorentzian humps of NI and pristine SBD at low forward bias and low temperatures.

Table 2
Extracted parameters for NI and pristine SBDs.

	T (K)	A ($\times10^{-23}$)	τ (ms)	B ($\times10^{-25}$)
NI	50	1.66	2.53	2.94
	77	1.74	2.32	2.24
	100	2.06	2.55	2.49
	120	2.25	2.63	2.30
Pristine	50	0.41	2.91	0.67
	77	0.41	2.89	0.70
	100	0.48	3.14	0.65
	120	0.49	3.16	1.02

(NPSD) of the two SBDs were typically at the same level at low temperature of 50 K. As increasing the temperature, the noise level of NI-SBD was still kept low, about two orders of magnitude lower than the pristine sample at 350 K. The lowered noise level was believed to be associated with the reduced leakage current, particularly at high temperatures. Different from the reverse-biased case, data collected at a low forward bias (0.2 V) reflected that the NI-sample exhibited a relatively higher total noise level than the pristine counterpart, as shown in Fig. 5 (b). The low-frequency regime noise consists of flicker noise superimposed with a Lorentzian shape, which is the characteristic of the generation-recombination (G-R) process. Parameters of Lorentzian humps and *1/f* noise could be separately extracted from Eq. (5) below [49,50].

$$S_I = \frac{A\tau}{1 + (2\pi f\tau)^2} + \frac{B}{f} \quad (5)$$

where S_I is the low-frequency noise power spectral density of devices. A, B determine the magnitude of Lorentzian hump and $1/f$ noise, respectively. τ is the time constant of each G–R center. Extracted results of A, B and τ for NI and pristine diodes are shown in Table 2. From 50 K to 120 K, distinct Lorentzian humps were observed in addition to a larger constant B value, the average time constant τ of the NI-sample was found around 17.2% smaller than that of the pristine sample, indicating a more active generation-recombination process in the NI-sample despite a low carrier injection level. And the active generation-recombination process was believed to be linked with high trap concentration of deep-level trap E4 as well as of E1 &E2.

4. Conclusion

In summary, temperature-dependent electrical characterizations were performed for a 14.9 MeV neutron-irradiated GaN SBD, employing *C-V-T*, *I-V-T*, *DLTS,* and *LFNS* measurements. *C-V* measurements revealed a greatly reduced carrier concentration inside the NI diode and a thermal-enhanced carrier removal effect. The forward conduction was relatively compromised for the NI-diode and a two-barrier model was employed to describe the barrier height inhomogeneity of the NI sample. Slight decrease of mean leakage current was identified for the NI-sample and trap-assisted Poole-Frenkel emission could well explain the leakage mechanism. In addition to increased trap concentrations for shallow traps E1 and E2, a new deep-level trap was revealed for the NI-diode by capacitance-based *DLTS*. As a result of low reverse current, the NI-sample demonstrated a lower frequency noise level when reverse biased. However, a more active G-R process, as reflected by the Lorentzian humps, was identified and linked to newly-generated deep-level trap E4 as well as E1&E2 with increased trap concentration. The vigorous characteristics indicated that GaN SBDs are promising for applications demanding high resistance to neutron irradiations and outstanding robustness in cryogenic temperatures.

CRediT authorship contribution statement

Min Zhu: Investigation, Methodology, Formal analysis, Data Curation, Writing - Original Draft, Writing - Review & Editing, Visualization.
Yuan Ren: Methodology, Investigation.
Leidang Zhou: Methodology, Investigation.
Jiaxiang Chen: Formal analysis, Investigation, Writing - Review & Editing.
Haowen Guo: Formal analysis, Investigation, Writing - Review & Editing.
Liqi Zhu: Methodology, Investigation.
Baile Chen: Methodology, Discussion.
Liang Chen: Methodology, Discussion.
Xing Lu: Formal analysis, Investigation, Writing - Review & Editing.
Xinbo Zou: Conceptualization, Methodology, Writing - Original Draft, Writing - Review & Editing, Validation, Supervision, Project administration, Funding acquisition.

Declaration of competing interest

The authors declare that they have no known competing financial interests or personal relationships that could have appeared to influence the work reported in this paper.

Acknowledgments

This work was supported in part by ShanghaiTech University Startup Fund, in part by the Shanghai Pujiang Program under Grant 18PJ1408200, and in part by the Shanghai Eastern Scholar (Youth) Program.

Appendix A. Supplementary data

Supplementary data to this article can be found online at https://doi.org/10.1016/j.microrel.2021.114345.

References

[1] A. Floriduz, J.D. Devine, Microelectron. Reliab. 110 (2020), 113656.
[2] A.C. Vilas Bôas, M.A.A. de Melo, R.B.B. Santos, R. Giacomini, N.H. Medina, L. E. Seixas, S. Finco, F.R. Palomo, A. Romero-Maestre, M.A. Guazzelli, Microelectron. Reliab. 116 (2021), 114000.
[3] Z. Islam, A.L. Paoletta, A.M. Monterrosa, J.D. Schuler, T.J. Rupert, K. Hattar, N. Glavin, A. Haque, Microelectron. Reliab. 102 (2019), 113493.
[4] C. Sharma, A.K. Visvkarma, R. Laishram, A. Kumar, D.S. Rawal, S. Vinayak, R. Singh, Microelectron. Reliab. 105 (2020), 113565.
[5] Helen M.O. Parker, Mauro Licata, Frank D. Cave, Michael D. Aspinall, Malcolm J. Joyce, Manuel S. Bandala, Domas Gerta, S. Conway, Presented at 2018 IEEE Nuclear Science Symposium and Medical Imaging Conference (NSS/MIC), 2018.
[6] X.M. Chen, Z.L. Ren, J.G. Zhang, C. Zheng, B.S. Tan, C.D. Yang, S.J. Chu, Plasma Sci. Technol. 11 (2009) 368.
[7] L. Paredes, R. Genis, M. Balcazar, L. Tavera, E. Camacho, Radiat. Meas. 31 (1999) 475–478.
[8] Q.-Y. Wang, J.-H. Wang, H.-F. Deng, L.-Y. Lin, Microelectron. Eng. 66 (2003) 333.
[9] F. Roccaforte, P. Fiorenza, G. Greco, R. Lo Nigro, F. Giannazzo, F. Iucolano, M. Saggio, Microelectron. Eng. 187–188 (2018) 66.
[10] R.K. Kaneriya, G. Rastogi, P.K. Basu, R.B. Upadhyay, A.N. Bhattacharya, Microelectron. Eng. 233 (2020), 111433.
[11] A.Y. Polyakov, S.J. Pearton, P. Frenzer, F. Ren, L. Liu, J. Kim, J. Mater. Chem. C 1 (2013) 877.
[12] J. Xu, R. Wang, L. Zhang, S. Zhang, P. Zheng, Y. Zhang, Y. Song, X. Tong, Appl. Phys. Lett. 117 (2020), 023501.
[13] M. Ahmed, B. Kucukgok, A. Yanguas-Gil, J. Hryn, S.A. Wender, Radiat. Phys. Chem. 166 (2020), 108456.
[14] E. Gaubas, T. Ceponis, L. Deveikis, D. Meskauskaite, S. Miasojedovas, J. Mickevicius, J. Pavlov, K. Pukas, J. Vaitkus, M. Velicka, M. Zajac, R. Kucharski, J. Phys. D. Appl. Phys. 50 (2017), 135102.
[15] A. Sandupatla, S. Arulkumaran, N.G. Ing, S. Nitta, J. Kennedy, H. Amano, Micromachines (Basel) 11 (2020).
[16] A. Sandupatla, S. Arulkumaran, K. Ranjan, G.I. Ng, P.P. Murmu, J. Kennedy, S. Nitta, Y. Honda, M. Deki, H. Amano, Sensors (Basel) 19 (2019).
[17] S. Arulkumaran, K. Ranjan, G.I. Ng, J. Kennedy, P.P. Murmu, T.N. Bhat, S. Tripathy, J. Vac. Sci. Technol., B: Nanotechnol. Microelectron.: Mater., Process., Meas., Phenom. 34 (2016).
[18] E.J. Katz, C.-H. Lin, J. Qiu, Z. Zhang, U.K. Mishra, L. Cao, L.J. Brillson, J. Appl. Phys. 115 (2014), 123705.
[19] K. Lorenz, J.G. Marques, N. Franco, E. Alves, M. Peres, M.R. Correia, T. Monteiro, Nucl. Instrum. Methods Phys. Res., Sect. B 266 (2008) 2780.
[20] C.-H. Lin, E.J. Katz, J. Qiu, Z. Zhang, U.K. Mishra, L. Cao, L.J. Brillson, Appl. Phys. Lett. 103 (2013), 162106.
[21] J.G. Marques, K. Lorenz, N. Franco, E. Alves, Nucl. Instrum. Methods Phys. Res., Sect. B 249 (2006) 358.
[22] K. Kuriyama, M. Ooi, A. Onoue, K. Kushida, M. Okada, Q. Xu, Appl. Phys. Lett. 88 (2006), 132109.
[23] A.Y. Polyakov, N.B. Smirnov, A.V. Govorkov, A.V. Markov, N.G. Kolin, D. I. Merkurisov, V.M. Boiko, K.D. Shcherbatchev, V.T. Bublik, M.I. Voronova, S. J. Pearton, A. Dabiran, A.V. Osinsky, J. Vac. Sci. Technol., B: Microelectron. Nanometer Struct.–Process., Meas., Phenom. 24 (2006) 2256.
[24] V.N. Brudnyi, V.M. Boiko, N.G. Kolin, A.V. Kosobutsky, A.V. Korulin, P.A. Brudnyi, V.S. Ermakov, Semicond. Sci. Technol. 33 (2018), 095011.
[25] A.Y. Polyakov, N.B. Smirnov, A.V. Govorkov, A.V. Markov, E.B. Yakimov, P. S. Vergeles, N.G. Kolin, D.I. Merkurisov, V.M. Boiko, I.-H. Lee, C.-R. Lee, S. J. Pearton, J. Electron. Mater. 36 (2007) 1320.
[26] Y. Ren, L. Zhou, K. Zhang, L. Chen, X. Ouyang, Z. Chen, B. Zhang, X. Lu, Phys. Status Solidi A 217 (2019) 1900701.
[27] L. Lv, P. Li, X. Ma, L. Liu, L. Yang, X. Zhou, J. Zhang, Y. Cao, Z. Bi, T. Jiang, Q. Zhu, Y. Hao, IEEE Trans. Nucl. Sci. 64 (2017) 643.
[28] W. Gu, X. Xu, L. Zhang, Z. Gao, X. Hu, Z. Zhang, Crystals 8 (2018) 198.
[29] L. Lv, X. Yan, Y. Cao, Q. Zhu, L. Yang, X. Zhou, X. Ma, Y. Hao, IEEE Trans. Nucl. Sci. 66 (2019) 886.
[30] M. Mikelsen, U. Grossner, J.H. Bleka, E.V. Monakhov, B.G. Svensson, R. Yakimova, A. Henry, E. Janzén, A.A. Lebedev, Mater. Sci. Forum 600–603 (2008) 425.
[31] M. Higashiwaki, K. Konishi, K. Sasaki, K. Goto, K. Nomura, Q.T. Thieu, R. Togashi, H. Murakami, Y. Kumagai, B. Monemar, A. Koukitu, A. Kuramata, S. Yamakoshi, Appl. Phys. Lett. 108 (2016).
[32] J.H. Werner, H.H. Güttler, J. Appl. Phys. 73 (1993) 1315.
[33] E.I. Shabunina, M.E. Levinshtein, N.M. Shmidt, P.A. Ivanov, J.W. Palmour, Solid State Electron. 96 (2014) 44.
[34] V. Kumar, A.S. Maan, J. Akhtar, Mater. Sci. Semicond. Process. 115 (2020), 105108.
[35] N. Allen, T. Ciarkowski, E. Carlson, L. Guido, Semicond. Sci. Technol. 34 (2019), 095003.
[36] C. Raynaud, K. Isoird, M. Lazar, C.M. Johnson, N. Wright, J. Appl. Phys. 91 (2002) 9841.
[37] J. Chen, M. Zhu, X. Lu, X. Zou, Appl. Phys. Lett. 116 (2020), 062102.
[38] S. Karadeniz, M. Ahin, N.Tu Luo Lu, H. Afak, Semicond. Sci. Technol. 19 (2004) 1098.
[39] J.H. Werner, H.H. Güttler, J. Appl. Phys. 69 (1991) 1522.
[40] J.P. Sullivan, R.T. Tung, M.R. Pinto, W.R. Graham, J. Appl. Phys. 70 (1991) 7403.
[41] Q. Zhou, R. Zheng, J. Wang, B. Li, H. Wu, H. Li, X. Tang, Z. Qin, D. Dong, Y. Lin, C. Lu, R. Qiu, IEEE J. Electron Devices Soc. 7 (2019) 662.
[42] K.R. Peta, B.-G. Park, S.-T. Lee, M.-D. Kim, J.-E. Oh, T.-G. Kim, V.R. Reddy, Thin Solid Films 534 (2013) 603.
[43] Y. Zhang, J. Zhang, H. Zhou, T. Zhang, H. Wang, Z. Feng, Y. Hao, Solid State Electron. 169 (2020), 107807.
[44] W. Chikhaoui, J.M. Bluet, M.A. Poisson, N. Sarazin, C. Dua, C. Bru-Chevallier, Appl. Phys. Lett. 96 (2010), 072107.
[45] C.H. Chen, R. Sadler, D. Wang, D. Hou, B. Ou, 2017 IEEE Compound Semiconductor Integrated Circuit Symposium (CSICS), 2017.
[46] Z. Zhang, C.A. Hurni, A.R. Arehart, J.S. Speck, S.A. Ringel, Appl. Phys. Lett. 101 (2012), 152104.
[47] A.R. Arehart, A. Corrion, C. Poblenz, J.S. Speck, U.K. Mishra, S.A. Ringel, Appl. Phys. Lett. 93 (2008), 112101.
[48] Z. Zhang, E. Farzana, W.Y. Sun, J. Chen, E.X. Zhang, D.M. Fleetwood, R. D. Schrimpf, B. McSkimming, E.C.H. Kyle, J.S. Speck, A.R. Arehart, S.A. Ringel, J. Appl. Phys. 118 (2015), 155701.
[49] A. Kumar, V. Kumar, R. Singh, J. Phys. D. Appl. Phys. 49 (2016) 47lt01.
[50] L. Zhu, J. Huang, Z. Xie, Z. Deng, L. Chen, C. Lin, B. Chen, IEEE Trans. Electron Devices 67 (2020) 547.